Probing excited electronic states and ionisation mechanisms of fullerenes

Post-print of a peer-reviewed article published by the Royal Society of Chemistry.
Published article available at: http://dx.doi.org/10.1039/C3CS60047E

Cite as:
Johansson, J. O., & Campbell, E. E. B. (2013). Probing excited electronic states and ionisation mechanisms of fullerenes. *Chemical Society Reviews*, 42(13), 5661-5671.

Manuscript received: 05/02/2013; Article published: 23/04/2013

Probing excited electronic states and ionisation mechanisms of fullerenes**†

J. Olof Johansson[1] and Eleanor E. B. Campbell[1,*]

[1]EaStCHEM, School of Chemistry, Joseph Black Building, University of Edinburgh, West Mains Road, Edinburgh, EH9 3JJ, UK.

[*]Corresponding author; e-mail: Eleanor.Campbell@ed.ac.uk, fax: +44 (0)1316506453, tel: +44 (0)1316504729

[**]We gratefully acknowledge the contribution of a large number of collaborators to the work presented here, in particular Francoise Remacle, Benoit Mignolet, Klavs Hansen and Juraj Fedor. Financial support was provided from the Leverhulme Foundation (RPF-298 "PES of hollow nanomaterials").

[†]Celebrating 300 years of Chemistry at Edinburgh.

Abstract:
Fullerenes are interesting model systems for probing the complex, fundamental electron dynamics and ionisation mechanisms of large molecules and nanoparticles. In this Tutorial Review we explain how recent experimental and theoretical advances are providing insight into the interesting phenomenon of thermal electron emission from molecular systems and the properties of hydrogenic, diffuse, excited electronic states, known as superatom molecular orbitals, which are responsible for relatively simple, well-resolved structure in fs laser photoelectron spectra of fullerenes. We focus on the application of velocity map imaging combined with fs laser photoionisation to study angular-resolved photoelectron emission.

Graphical abstract:

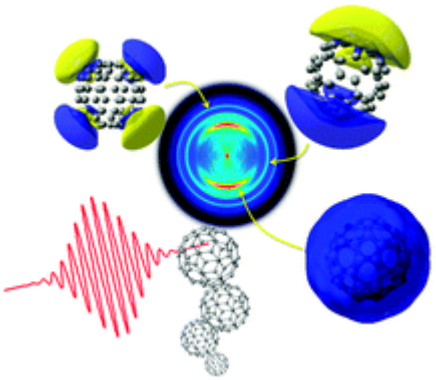

Introduction

Fullerenes are beautifully simple, complex molecules. This may sound like a contradiction in terms. However, due to their highly symmetrical nature (C_{60} is one of very few covalently bonded molecules with icosahedral, I_h symmetry) and their elemental purity, fullerenes are very convenient and interesting model systems to study and understand the fundamental, dynamical properties of large, complex molecules. Their discovery in 1985[1] and "mass production" and purification in 1990[2] also arguably heralded the onset of the rapid development of nanoscience as a distinct scientific discipline. Fullerenes can also be considered as archetypical nanoscale "building blocks" and show properties that often appear to lie between those of molecules and bulk materials. For this reason their early "home" was in the discipline of cluster science that studies the fundamental properties of matter on the nanoscale and how the bulk properties emerge as the size is increased, atom by atom or molecule by molecule. The fundamental properties of fullerenes still continue to surprise and fascinate, as we hope will be clear from the following Tutorial Review. However, much of the focus of fullerene research worldwide now lies in the development of fullerene-based materials for organic photovoltaic applications[3]. The spectacular increase in efficiency of fullerene-based solar cells from 1% to over 9% within a decade makes them serious contenders for large scale commercialisation. Large molecules such as fullerenes and conjugated hydrocarbon systems are also promising materials for use in molecular electronics[4]. An understanding of the excited state properties and of the electron dynamics upon light excitation is important in order to optimise charge transport phenomena in devices that could be used in optoelectronics or organic solar cells. The interaction of large molecules with ultrafast laser fields and the subsequent electron dynamics is also of fundamental importance to understand the possibilities and limitations of coherent control.[5] Understanding and controlling electron dynamics and de-coherence of large organic molecules is a challenge[6] but could be of far-reaching importance for the future development of low-cost, efficient, flexible, light-weight electronic components and even molecular logic applications.[7] Fullerenes are very suitable model molecular systems for exploring the fundamental electron dynamics and competing relaxation processes in large

molecules[8] and for developing predictive theoretical tools to help in the design and development of practical molecular materials.

This review treats recent advances in understanding the multi-photon ionisation behaviour of gas-phase fullerenes, and related systems. In particular, results obtained using angular resolved photoelectron spectroscopy will be discussed. After a brief overview of experimental methods, we start by describing the thermal ionisation behaviour that is observed from fullerenes and other systems that have a combination of high electronic density of states, high atomic binding energies and low ionisation energies.[8] When ns laser pulses are used to excite the molecules, the high density of states and very efficient energy coupling within the molecule leads to the incoherent absorption of many photons and a rapid increase in the vibrational temperature. One therefore predominantly observes thermionic electron emission from the vibrationally excited molecules.[8-10] We will briefly describe how we model this behaviour and how the situation changes as the timescale for excitation is decreased below the timescale for electronic to vibrational energy coupling.[11] When ionising small molecules with fs laser pulses, one often sees a relatively simple photoelectron spectrum (PES) that consists of a few prominent peaks that are due to single-photon ionisation of low-lying Rydberg states. [12-14] Similar features are seen in fs laser PES of fullerenes[15, 16] superimposed on a background of thermal electrons.[17, 18] We will discuss the interesting nature of these states in fullerenes and the reason for their prominence in the PES.[16]

Experimental Techniques

Gas-Phase Fullerenes

In order to study fullerenes in the gas-phase, one has to sublime the solid material because the vapour pressure is very low at room temperature. Typically a temperature around 350 - 500 °C is needed to produce a sufficient density of fullerenes in a molecular beam to carry out gas-phase spectroscopy.

Commercial fullerene powder is typically placed in a small oven with an aperture of a few mm diameter, separated from the interaction region by a skimmer. It is important to ensure that remaining solvent or other impurities are removed before any spectroscopy experiments are carried out. This is usually done by heating the material overnight in high vacuum at a temperature of 100-200 ^{o}C. This is sufficient for the photoionisation experiments that are the subject of this review and where the mass spectrum will clearly indicate the presence of any unwanted species that may influence the measured PES. For more sensitive studies it is necessary to first carefully purify the material by sublimation in the absence of oxygen.[19] The high temperature needed to sublime the fullerenes may be considered to be problematic for obtaining spectroscopic information, however, it does not adversely affect the resolution of the peak structure in the fs PES, as will be discussed later. It is possible to produce fullerene beams that have low vibrational temperatures by using collisional cooling with He, either in a Smalley-type laser desorption source[20] or by using a cluster-aggregation type source.[21] Such approaches have been used to obtain high resolution resonant-enhanced two-photon ionisation spectra of low-lying excited valence states where time is allowed for the initial resonantly excited state to couple to the triplet manifold. The second, ionisation step involves single-photon ionisation from the lowest lying triplet state.[20] Another way of obtaining, and spectroscopically probing, vibrationally cold fullerenes is to embed them in liquid He droplets.[22] The results discussed in this article have all been obtained with high temperature molecular beams.

Detection of Charged Particles

Inside a vacuum chamber, the effusive molecular beam is intersected by a laser at right angles in order to excite and ionise the fullerenes. An example of a typical setup is shown in Figure 1(a). The resulting positively charged ions and the emitted electrons are detected using a combination of time-of-flight mass spectrometry and photoelectron spectroscopy. Early studies of multiphoton ionisation used conventional time-of-flight photoelectron spectrometers.[15] In recent years, the advance of velocity-map imaging[23] (Figure 1b) has greatly improved the possibilities for angular resolved photoelectron spectra to be recorded, and has brought some new insights that will be the main focus

of the discussions in this article. The interaction region of the molecules and the laser is situated inside an electrode assembly that allows for the ions to be extracted into a TOF mass spectrometer and/or the photoelectrons to be detected on a position sensitive detector consisting of a pair of

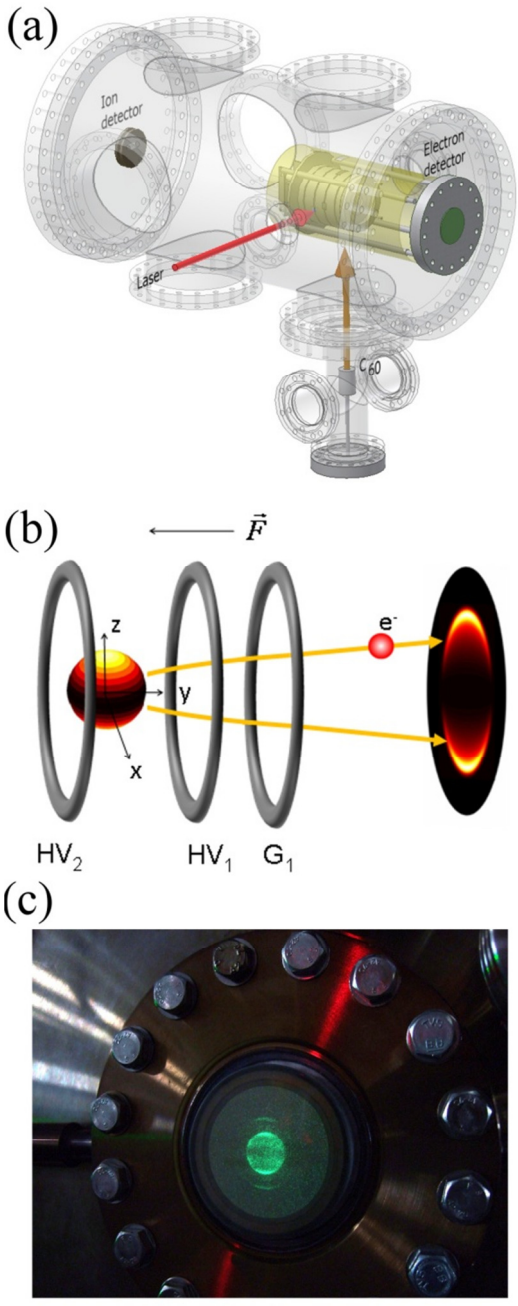

Figure 1: *(a) Typical experimental setup for studying laser photoionisation of gas-phase fullerenes. Molecules are produced in an effusive oven situated in the lower vacuum chamber. Sublimed molecules are intersected by the laser in the upper chamber. Ions are extracted towards the ion detector and electrons towards the position-sensitive detector. (b) VMI. Photoelectrons are created at the origin and extracted towards a position sensitive detector (in the xz-plane) with a static electric field (**F**). The field is applied using three electrodes HV_2, HV_1 and G_1. The laser propagates along the x-axis and the polarisation direction is parallel with the z-axis. The sphere between HV_2 and HV_1 illustrates a spatial distribution, aligned along the laser polarisation direction, of outgoing photoelectrons with the same kinetic energy after ionisation. The detected projection is shown on the detector to the right in the image. (c) Photo of a position sensitive detector consisting*

microchannel plates and a phosphor screen, Figure 1(c). The electrons can be extracted in a way that

allows for velocity map imaging (VMI)[5] so that electron kinetic energy and angular distributions can be recorded simultaneously.

When used in the VMI configuration, the electrodes act as an electrostatic lens. No meshes are used, resulting in a spatial focusing of the electrons such that photoelectrons with the same initial momentum, whether or not they are produced at the same point in space, will arrive at the same spot on the detector.[24] It is necessary to "reconstruct" the original 3D electron distribution by applying an inverse Abel transform to the detected 2D distribution. Various procedures are available to do this such as BASEX[25], p-BASEX[26] and POP[27], each of which has particular advantages and disadvantages. It is advisable to check the results for consistency using more than one inversion procedure.

Rydberg Fingerprint Spectroscopy

Many molecules show characteristic peaks in fs laser photoelectron spectra (PES) that are attributed to single-photon ionisation of low-lying members of Rydberg series. Multiphoton excitation followed by efficient internal conversion can populate a series of excited Rydberg states with differing amounts of vibrational excitation. Within the same ca. 100 fs duration laser pulse, the absorption of an additional photon will lead to ionisation. In spite of the varying amounts of vibrational excitation and the sometimes high vibrational temperature of the neutral molecule, the peaks due to ionisation from these states are well-defined and the binding energies can be determined accurately. This is because there is a strong propensity for $\Delta v = 0$ transitions in the final, ionising step due to the structural similarity of the Rydberg states and the cation.[14] Since these low-lying Rydberg states penetrate the core region of the molecule, their detected binding energies are influenced by the core structure.[14] When combined with mass spectra, the fs laser PES provides a means of distinguishing between molecular isomers. For this reason, the technique is known as Rydberg Fingerprint Spectroscopy. Since one can consider the influence of the core potential as changing the phase of the hydrogenic Rydberg electron wavefunction, the technique has been likened to electron diffraction.[28] Although the excited states that contribute to the structure shown in the fullerene fs PES are not strictly speaking

pure Rydberg states, as will be discussed later, they are also diffuse orbitals that can be thought of as low-lying members of Rydberg series and the mechanisms for their population and detection appear to be very similar. The electron binding energies in the excited states are obtained directly from the PES by assuming that the final ionisation step is a single-photon ionisation and also assuming that Koopman's theorem holds, giving, the relationship $E_{\mathrm{Bind}} = h\nu - E_{\mathrm{Kin}}$, where E_{Bind} is the electron binding energy in the excited state, $h\nu$ is the photon energy and E_{Kin} is the experimentally determined electron kinetic energy. This is illustrated in Figure 2(a).

Angular-Resolved Photoelectron Spectroscopy

The VMI technique is a relatively simple, but powerful technique to measure photoelectron angular distributions (PADs). The emission direction is measured with respect to the direction of the linearly polarised electric field of the laser used to ionise the sample. The angular distribution from a given initial state, assuming a one-photon ionisation process from a randomly oriented sample, is given by [29]

$$I(\theta) = \frac{\sigma_{total}}{4\pi}\left(1 + \beta \mathrm{P}_2(\cos\theta)\right) \qquad (1)$$

where σ_{total} is the angle-integrated cross-section, β is the anisotropy parameter ($-1 \leq \beta \leq 2$) and P_2 is the second order Legendre polynomial. For systems where the orbital angular momentum quantum number, ℓ, is a good quantum number, the anisotropy parameter, β, can be calculated according to[29]

$$\beta = \frac{\ell(\ell-1)R_{\ell-1}^2 + (\ell+1)(\ell+2)R_{\ell+1}^2 - 6\ell(\ell+1)R_{\ell+1}R_{\ell-1}\cos\left(\delta_{\ell+1} - \delta_{\ell-1}\right)}{(2\ell+1)(\ell R_{\ell-1}^2 + (\ell+1)R_{\ell+1}^2)}, \qquad (2)$$

where $R_{\ell\pm1} = \int \psi_f^{\ell\pm1}(r)\psi_i^{\ell}(r)r^3 dr$ are the radial dipole matrix elements involving the final (f) and initial (i) states. The wavefunction for the outgoing electron, which is included in the final state, will change its radial dependence depending on the electron's momentum. This means that $R_{\ell\pm1}$ will change with the kinetic energy of the photoelectron, which in turn means that β can change with kinetic energy. It is therefore useful to study β for a range of electron kinetic energies by varying the

wavelength of the ionising laser (Figure 2(b)). This dependence can then be compared to calculations, and in combination with binding energies, one can use this information to assign peaks in the photoelectron spectra and also provide a rigid test of the predictions of theoretical calculations. There is one exception for the β-value's dependence on electron kinetic energy. For $\ell = 0$, the outgoing electron wave can only be a pure *p*-wave and therefore, in the absence of strong perturbing effects, $\beta = 2$. The subject of PADs has been discussed extensively in the literature and we refer to two recent reviews for a more detailed discussion.[30, 31]

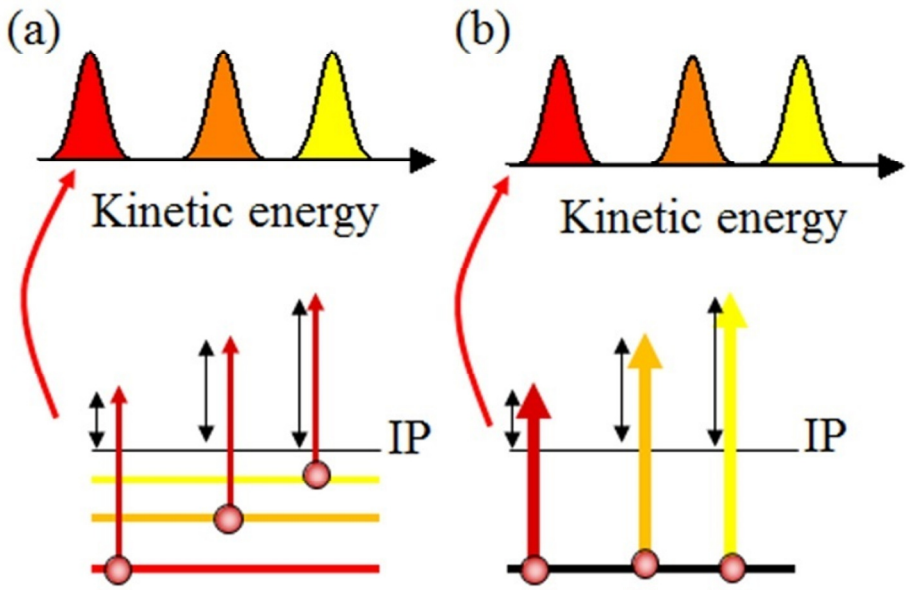

Figure 2: *Illustration of PES. In (a), a range of states populated are one-photon ionised producing a series of peaks for which their kinetic energy can be converted to binding energy. (b) By varying the ionising wavelength, the kinetic energy of an electron from a specific state changes and it is possible to determine the kinetic energy dependence of the anisotropy parameter from the photoelectron angular distributions. IP indicates the ionisation potential of the molecule.*

The information from angular distributions gives an interesting compliment to conventional photoelectron spectroscopy. In addition to the study of electrons produced via single-photon ionisation from distinctive excited states, angular distributions from electrons emitted through processes other than single-photon ionisation produce particular features in PES. Examples are thermally emitted electrons (covered in this review) but also electrons produced from field ionisation that are re-collided with the parent molecules and give the opportunity to study laser-induced electron diffraction.[32 33]

Thermal Electron Emission from Fullerenes after Laser Excitation

In this section, thermal electron emission will be introduced and the two limiting cases when exciting with ns or fs pulses will be discussed.

Ns Laser Excitation of C_{60}

Some of the earliest studies of laser photoionisation of purified fullerene beams using time-of-flight mass spectrometry (TOF) showed the presence of a long tail on the parent ion peak extending to longer timescales.[9] A typical example of a photoionisation/fragmentation spectrum obtained from C_{60} using ns laser pulses is shown in Figure 3(a). The tail was shown to be due to ionisation from the parent molecule occurring on the timescale of microseconds, i.e. much later than the duration of the laser pulse. Similar behaviour was observed at about the same time when studying refractive metal clusters[34] and has since been observed for many anionic systems, down to quite small molecules. [35] Delayed ionisation is seen for systems where the ionisation potential (or electron affinity) is low, the dissociation energy for the molecule is high and the laser photon energy is less than the ionisation potential (in the case of the fullerenes, less than the energy needed to photoionise the lowest triplet state).[8] The mechanism is considered to be akin to thermionic emission of electrons from hot metals. For ns laser pulses, the energy is absorbed at such a relatively low rate that the electronic excitation is quickly coupled to vibrationally excited states while photons continue to be absorbed during the ns

pulse. The combination of a high density of states and a strong coupling between electronic and vibrationally excited states, provides favourable conditions for the excitation energy to be quickly equilibrated among all degrees of freedom, and this is what is typically assumed. There has been some discussion in the literature over the past thirty years as to whether the delayed electron emission from fullerenes can be considered to be truly thermionic (i.e. completely statistical) or not. However, a completely statistical description, based on detailed balance arguments, does seem to be consistent with the majority of experimental observations if the experimental internal energy distributions and competition with other statistical decay processes are correctly taken into consideration.[36] A recent textbook[37] gives a comprehensive treatment of the detailed balance approach to describing statistical decay of nanoparticles based on the Weisskopf formalism and that is the approach normally used to describe the statistical decay behaviour of fullerenes and other atomic clusters.[10] This is predominantly a density of states argument, similar to the transition state theory (RRKM) approach more familiar to chemists. The difference lies in the treatment of the frequency factor that multiplies the ratio of level densities of the parent and daughter species. The Weisskopf formalism gives a rate constant for electron emission as a function of total internal energy, E, and electron kinetic energy, ε:

$$\begin{aligned} k(E,\varepsilon)d\varepsilon &= g\frac{m}{\pi^2\hbar^3}\sigma(\varepsilon)\varepsilon\frac{\rho_d(E-\Phi-\varepsilon)}{\rho_p(E)}d\varepsilon \\ &\cong 2\frac{m}{\pi^2\hbar^3}\sigma(\varepsilon)\varepsilon\frac{\rho_d(E)}{\rho_p(E)}\exp\left(\frac{-\Phi}{k_B T_p(E)}\right)\exp\left(\frac{-\varepsilon}{k_B T_d(E)}\right)d\varepsilon \end{aligned} \tag{3}$$

where g is the spin degeneracy (= 2), m is the electron mass, $\sigma(\varepsilon)$ is the cross section for the reverse process i.e. the capture of an electron by the daughter cation, $\rho_{d,p}$ are the densities of vibrational and electronic states for the daughter and parent species, respectively and Φ is the ionisation energy. T_p

and T_d are the microcanonical temperatures of the parent and daughter species, respectively.[ii] The capture cross section, $\sigma(\varepsilon)$, is usually estimated to be the classical capture probability for an electron in a Coulomb potential with a sticking coefficient of one, $\sigma(\varepsilon) = \pi r_0^2 (1 - V(r_0)/\varepsilon)$, where r_0 is the radius of the fullerene cage. The vibrational density of states can be calculated by using the Beyer-Swinehart algorithm[38] and vibrational energies for C_{60}. Accurate calculated values for the vibrational modes of C_{60} have been given by Giannozzi and Baroni[39]. For thermionic emission there is little contribution from excited electronic states and one usually just includes the ratio of the degeneracies of the ground states of the cation and neutral molecules. The model predicts an Arrhenius-type rate constant for the electron emission, $k(E) \cong A(E)\exp(-\Phi/k_B T_p(E))$, shown in Figure 4 for C_{60}, (with $A \approx 10^{15}$ s^{-1} and Φ = 7.6 eV) and also an exponentially decreasing emission probability with increasing electron kinetic energy, $I(\varepsilon) \propto \exp(-\varepsilon/k_B T_d)$, resembling a Boltzmann distribution. Bordas and co-workers have used velocity map imaging to study the time dependence of the PES under conditions in which thermionic emission is expected to take place.[40, 41] Their results clearly showed the thermal nature of the emission and provided important quantitative information for determining the Arrhenius parameters that describe the competing neutral fragmentation decay channel. An example of a ns laser C_{60} PES obtained using velocity map imaging is shown in Figure 3(b). One can clearly see the exponentially decreasing nature of the kinetic energy distribution as well as the isotropic distribution of electrons on the VMI image, as would be expected for a completely statistical emission mechanism.

[ii] An ensemble of molecules, with each molecule containing a fixed number of atoms and a fixed energy, E, i.e. isolated from a heat bath should be considered as a microcanonical ensemble, where the microcanonical temperature is defined as $k_B T = \left(\frac{d(\ln(\rho))}{dE}\right)^{-1}$.[37] Strictly speaking, the parent temperature, T_p, in eq.(3) should be calculated using the finite heat bath correction but this introduces only a minor correction.[17]

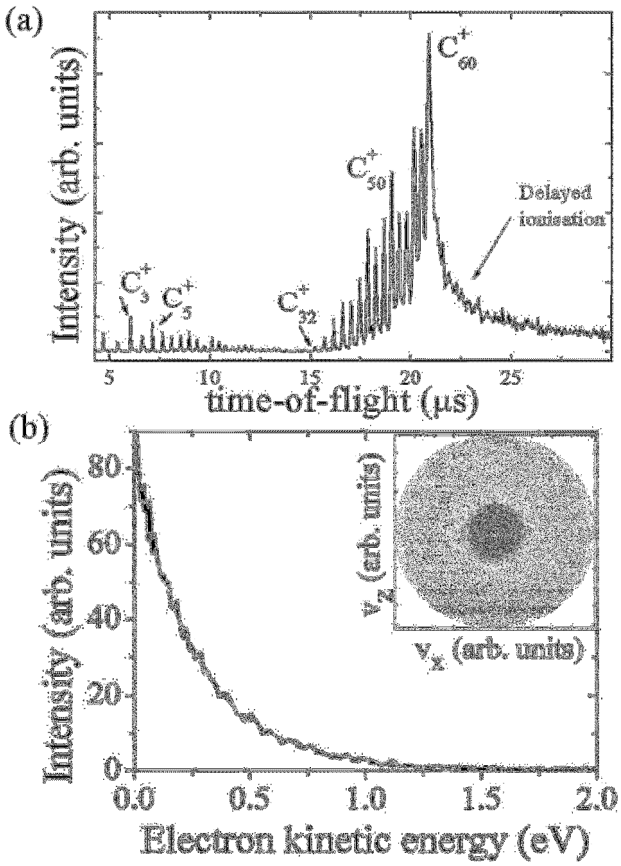

Figure 3: (a) *Time-of-flight mass spectrum obtained after ionising C_{60} using 4 ns pulses of 532 nm wavelength. The characteristic tail on the parent ion due to delayed, thermionic emission is clearly seen. (b) The PES for similar laser conditions is structureless and can be well-described using an exponential function. The inset shows the VMI image clearly illustrating an isotropic electron emission. Reprinted from J.O. Johansson, et al., EPJ Web of Conferences,* ***41****, 02015 (2013).*

Fs Laser Excitation of C_{60}

When using shorter, high intensity, laser pulses, on the order of 100 fs, the photon absorption rate is faster and multiple photons are absorbed before there is time for the coupling with vibrational degrees of freedom to take place. This influences the detected PES in two ways.[11] Firstly, structure appears in the spectrum that is very similar to that of Rydberg Fingerprint Spectroscopy. This is discussed in a later section. Secondly, a background signal of thermal electrons is still visible but the apparent

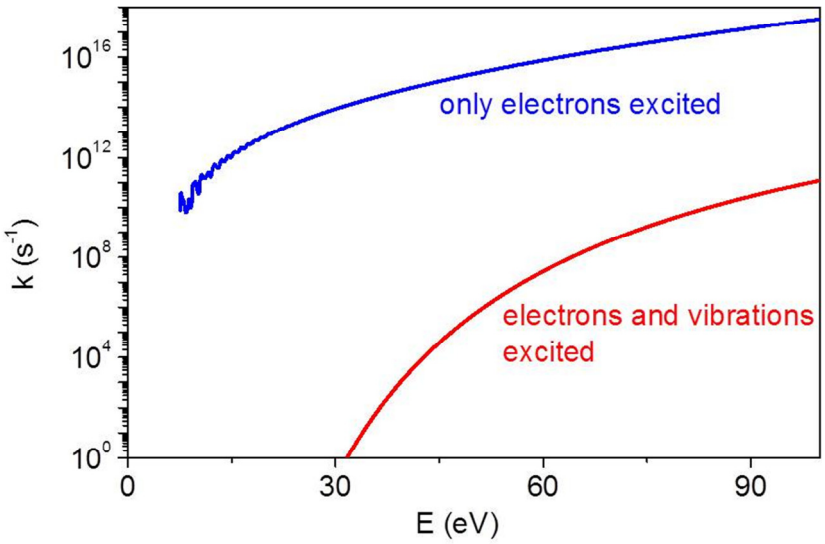

Figure 4. *Calculated rate constants for thermal electron emission from C_{60}. Upper curve: assuming energy equilibrated only among electronic degrees of freedom. Lower curve: assuming energy equilibrated between electronic and vibrational degrees of freedom, as in thermionic electron emission. Adapted from Hansen et al.*[17].

temperature of these electrons, determined by the reciprocal of the slope on a log-lin plot, is much higher than it is for the case of ionisation with ns laser pulses. An example is shown in Figure 5(a) for excitation with 400nm pulses of 120 fs duration. The isotropic nature of the thermal background emission is still clearly seen when comparing the PES along and perpendicular to the direction of laser polarisation. Another difference compared to ns excitation is that there are no signs of delayed ionisation in the TOF mass spectrum (Figure 5(b)). The different nature of the thermal electron emission under fs laser excitation can be explained by invoking what is effectively a two-temperature model.[17] We assume that the non-coherent excitation by absorption of multiple photons takes place on a timescale that is short compared to the electronic-vibrational coupling time. The absorbed energy is rapidly equilibrated among the electronic degrees of freedom and electrons can then be emitted thermally before equilibration with the vibrational degrees of freedom can take place. In other words

we consider hot electrons but cold vibrations. The theoretical model that is used to describe this is very similar to the Weisskopf formalism used for thermionic emission, as discussed above. The difference is that we confine the excitation energy to the electronic sub-system and need to consider the ratio of the electronic densities of states for the daughter and parent molecules. The electronic-vibrational coupling time is introduced as a means of removing excitation energy from the electronic

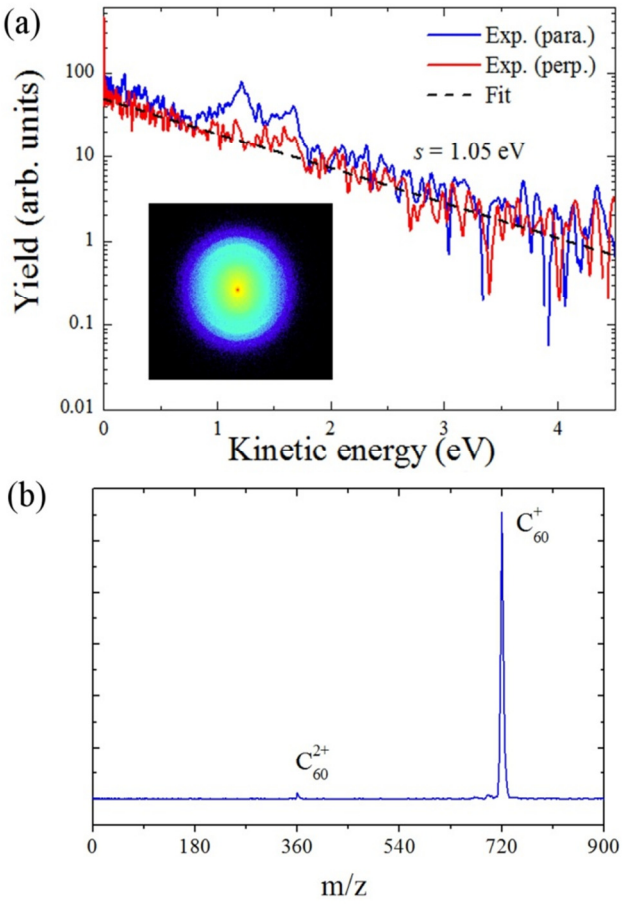

Figure 5: (a) *Angle-resolved PES along and perpendicular to the laser polarisation direction obtained after 400 nm, 120 fs laser excitation of 8x10^{11} Wcm^{-2} intensity. Note the logarithmic y-axis. The inset shows the corresponding VMI image, which is isotropic. Reproduced with permission from Journal of Chemical Physics* ***136****, 164301 (2012). Copyright 2012 American Institute of Physics.(b) The corresponding mass spectrum does not show the tail on the parent ion as is seen for delayed, thermionic emission induced by ns laser pulses (Fig. 3).*

sub-system on the timescale of a few 100 fs. The electronic density of states can be estimated using an algorithm given by Hansen et al.[17] Alternatively, a more simplified treatment can be adopted in which the total electronic level density is calculated from a simple Fermi gas single-particle level density, giving $\rho(E) \propto \exp\left(2\sqrt{aE}\right)$, with a = 29.7 eV^{-1} for C_{60}.[42] The lack of delayed ionisation visible in the TOF mass spectra can be explained by the much faster timescales for the thermal electron emission compared to the thermionic emission case observed with ns laser pulses. The calculated rate constants are ca. six orders of magnitude larger for the fs laser induced thermal emission than for thermionic emission for the same total excitation energy, Figure 4. The thermal background observed for excitation with fs lasers is thus also due to a delayed statistical ionisation mechanism but is too fast to be observed on the microsecond timescale detectable with a TOF mass spectrometer. The thermal, two-temperature transient hot electron model is able to explain many of the features of the fs PES of fullerenes, including the change in apparent temperature of the emitted

electrons with increasing laser fluence and the ion yields for different charge states as a function of laser fluence.[17]

Other mechanisms could also lead to a structureless Boltzmann-like distribution of photoelectron kinetic energies such as field ionisation, however the comparison between laser fluence and laser intensity dependence that was carried out by Kjellberg et al.[43] provided a convincing argument for the thermal nature of the emission. However, one initially concerning observation when VMI was first used for the electron detection threw some doubt on the thermal picture. When using 800 nm laser pulses of ca. 100 fs duration, the "thermal" electron background signal was seen to be anisotropic with an apparent "temperature" along the laser polarisation direction that appeared to be higher than the apparent temperature perpendicular to the polarisation direction.[18, 43] On reflection, this observation actually provided even more convincing evidence for the thermal, statistical nature of the electron emission.[18] Since the temperature cannot change with emission angle it appeared that the thermally emitted electrons were getting an extra "push" along the laser polarisation direction. The

asymmetry can be explained using classical electrodynamics where it is known that an electron "born" inside a transient time-varying electric field will be given a momentum kick from the field. The change in momentum is given by the instantaneous value of the vector potential of the field at the time of "birth". The kick is given by

$$eE_0/\omega \times \sin(\omega t_0)\mathbf{e}_z, \tag{4}$$

where –e is the electron's charge, E_0 is the electric field amplitude, ω is the laser angular frequency, t_0 is the time of emission and $\mathbf{e}_z$ is the unit vector along the polarization direction. When the electron is born at the peak of the vector potential (corresponding to zero instantaneous electric field), the maximum increase in electron kinetic energy is $2U_p$, where [18]

$$U_p(\text{eV}) = 9.34 \text{ x } 10^{-20} \times [\lambda(\text{nm})]^2 \times \text{I}(\text{Wcm}^{-2}), \tag{5}$$

is the ponderomotive energy. If an electron is born outside the temporal envelope of the time-varying field, no momentum kick will be imparted to the electron.

As shown in Figure 4, the electron emission rate is on the order of fs-ps when thermal electron emission from the electronic sub-system is considered. This can be seen more specifically in Figure 6(a), where a simple rate equation for the internal energy of the fullerenes was solved according to [18]

$$\frac{dE(t)}{dt} = \sigma_p I(t) - \frac{E(t)}{\tau}, \tag{6}$$

where $E(t)$ is the total excitation energy of the electrons, σ_P is the average photon absorption cross-section, $I(t)$ is the laser intensity and τ is the time constant for coupling to vibrations. The electron yield as a function of time,t, and electron excitation energy was then calculated using the Weisskopf formalism (Eq. 3) and compared to the timescale of the laser pulse duration[18]. The bulk of the thermally emitted electrons are seen to be emitted during the laser pulse, in contrast to thermionic emission where the electron emission takes place on a much longer timescale.

Electrons born at the peak of the electric field will not be given an extra momentum kick. This is the case for direct photoionisation which is why one can directly relate the photoelectron kinetic energy to the electron binding energy and why this does not change with increasing laser intensity. However, since the statistically-emitted thermal electrons are uncorrelated with the laser field, electrons can be born at any time and therefore be given an additional kinetic energy up to the maximum possible value of $2U_p$. The asymmetry is therefore seen to be a typical signature of thermally emitted electrons (Figure 7(b)).

Since the maximum momentum kick from the laser pulse is proportional to U_p, the asymmetry is wavelength dependent ($U_p \propto \lambda^2$, c.f. Equation 5). This is seen in Figure 7(a), where a clearly asymmetric electron kinetic energy distribution is observed after 800 nm excitation, in contrast to the results presented in Figure 5(a) for 400 nm excitation. The intensities are quite different, but the mass spectra and "perpendicular" apparent temperatures are similar, indicating that the same total amount of energy has been absorbed by the fullerenes. Note that it is only the thermal, background electrons that show the asymmetry, the kinetic energy of the electrons responsible for the peak structure superimposed on the thermal background, and discussed in more detail later, does not change with emission angle. The asymmetry can be characterised by comparing the difference, Δs, between the apparent temperature measured parallel and perpendicular to the laser polarisation direction (Figure 7a). When plotting Δs vs. U_p for 800 nm, it was found that the difference was close to $2U_p$, as can be seen in Figure 7(b). The time dependent electron yield was calculated, and, for each time step, the vector potential was found and the corresponding kick along the polarisation direction was given to the electrons emitted at that time step. The trend in asymmetry could be well reproduced using the

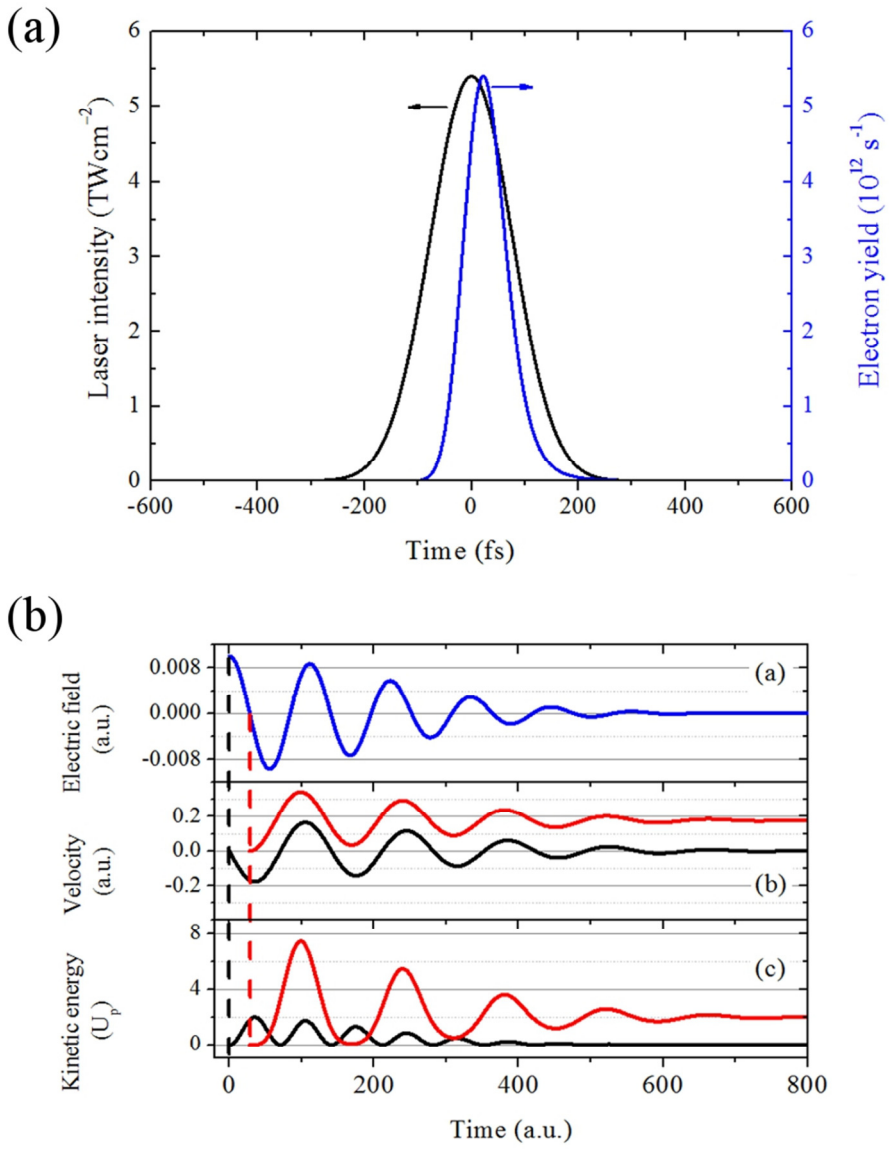

Figure 6: *(a) Calculated electron yield compared to the excitation laser envelope as a function of time for 180 fs, 800 nm, 5.4 TWcm^{-2}. Reprinted with permission from J. Chem. Phys.* ***136****, 164301 (2012). Copyright 2012 American Institute of Physics. (b) Influence of the laser electric field at "time of birth" on the kinetic energy of an emitted electron. Red: electrons emitted at zero oscillating electric field giving the maximum increase in kinetic energy of $2U_p$ along the polarisation direction. Black: an electron emitted at the peak of the oscillating laser field giving no net increase of electron kinetic energy.*

thermal emission model although the model underestimated the asymmetry for this example of 800nm excitation. In the model, not all electrons are emitted close to the maximum of the laser pulse envelope. This means that not all electrons will experience the full $2U_p$ kick and therefore a lower asymmetry than the maximum possible value is calculated. It is unclear why the data in this particular case show the maximum degree of asymmetry (results with other wavelengths, not yet published, show better agreement). It is possible that other effects, such as internal polarisation or re-collision effects may be contributing to the high asymmetry for excitation with 800 nm pulses.

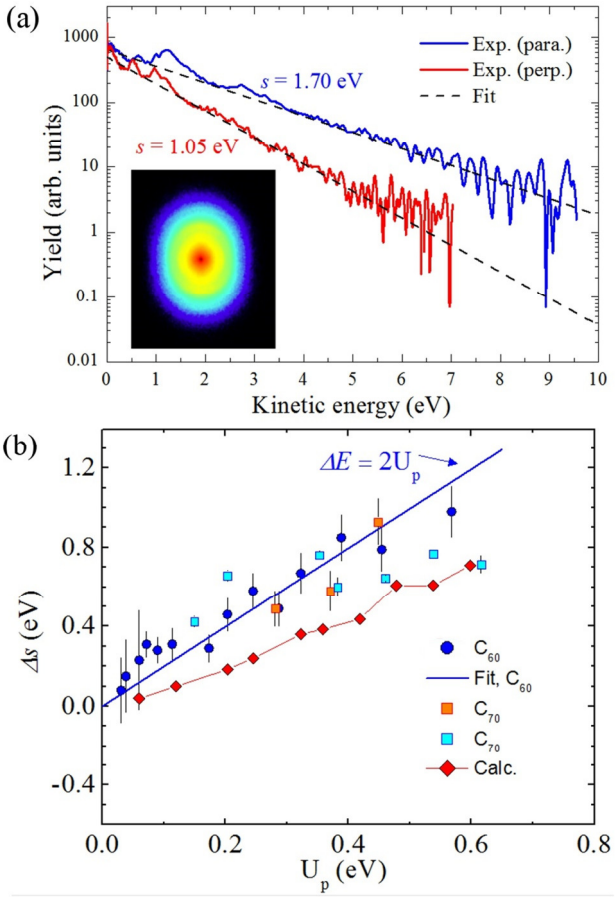

Figure 7: *(a) Angle-resolved PES from C_{60} along and perpendicular to the laser polarisation direction obtained after 800 nm, 180 fs laser excitation of 5.4 TWcm^{-2} intensity. There is clearly a difference in apparent temperature (inverse slope) along and perpendicular to the laser polarisation direction. The inset shows the VMI image, which is asymmetric. (b) The difference between parallel and perpendicular temperature as a function of the ponderomotive potential for a range of laser*

intensities and durations obtained using 800 nm. A fit was made and agrees surprisingly well with the maximum kick an electron can gain by being born inside a time-varying electric field. Model calculations obtained using a Monte-Carlo simulation are shown to reproduce the results reasonably well. Reprinted with permission from J. Chem. Phys. ***136****, 164301 (2012). Copyright 2012 American Institute of Physics.*

Fs-Laser-Induced Thermal Electron Emission in Other Systems

Experimental results, similar to the ones obtained for C_{60}, have been found for C_{70}[43] and the endohedral fullerene La@C_{82}[44], Figure 8. This supports the thermal model since material properties such as heat capacity are more relevant than the actual molecular structure that would be important for detailed spectroscopy. The endohedral molecules are of course similar to the empty fullerenes and so the results are perhaps not surprising. Experiments on cationic sodium clusters have also been interpreted by the transient thermal emission (or two-temperature) model[45,46] as have photoionisation studies of rare gas clusters[47]. Experiments have also been conducted identifying a similar ionisation mechanism for polycyclic aromatic hydrocarbons (PAHs)[48]. With increasing molecular size, a larger contribution from thermal electron emission was found. It is interesting to notice that the PAHs also show an asymmetric electron distribution, when ionised with 800nm, ca. 100 fs pulses, which further supports the hypothesis that the main electron emission channel for these laser conditions is thermal in nature. These results show that the occurrence of thermal electron emission from molecules under conditions of fs laser excitation may be more widespread than is generally believed and that this is a significant electron emission mechanism for molecular systems with high densities of states and efficient intramolecular couplings.

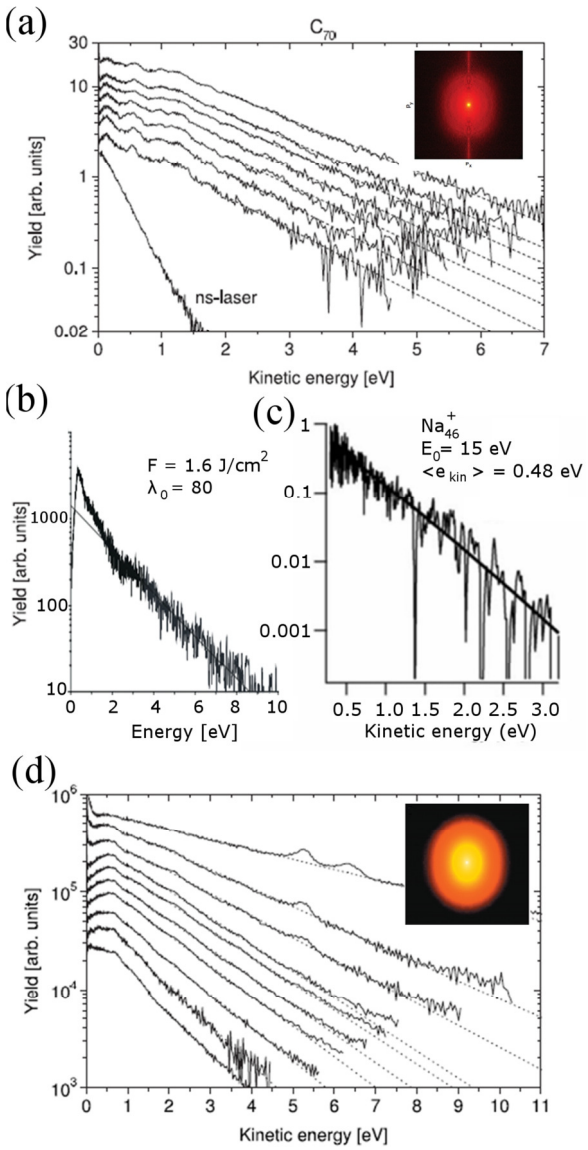

Figure 8: *Angle-integrated PES for (a) C_{70} obtained for various pulse durations and intensities ,reproduced with permission from Physical Review A* ***81,*** *023202 (2010), copyright (2010) by The American Physical Society (b) La@C_{82},, reproduced with kind permission from Springer Science+Business Media: Eur.Phys.J.D* ***34****,205 (2005), Fig. 5 (EDP Sciences, Società Italiana di Fisica, Springer-Verlag, 2005) (c) cationic Na_{46} clusters ,reprinted with permission from Elsevier from the Int. J. Mass Spectrom.* ***252*** *(2006) 157.(d) Coronene, reprinted with permission from Journal of Chemical Physics* ***133*** *(2010) 074308. Copyright (2010 American Institute of Physics..*

Observation of "Superatom-Molecular Orbitals" in Gas-Phase Fullerenes

We have previously discussed the thermal electron distributions seen in PES after fs laser excitation. We will now focus on the peak structure that is superimposed on the thermal background as seen e.g. in Figures 5 and 7. This peak structure can be quite sharp and clear, in contrast to what might be expected from a vibrationally hot molecule, that, in addition, shows thermal electron emission. The structure is related to the relatively simple spectra seen in Rydberg Fingerprint Spectroscopy and has a similar origin: single-photon, $\Delta v = 0$ transitions from a wide range of low-lying excited Rydberg-like states. The states that are probed in the fullerenes are not pure Rydberg states and have been given the name "Super Atom Molecular Orbitals" (SAMO) in order to stress the distinction.[49] The first observations of peak structures in fs PES of fullerenes were reported using a TOF photoelectron spectrometer and did not involve the determination of photoelectron angular distributions.[15] The peaks were assigned by solving the Schrödinger equation using a simple empirical jellium potential for C_{60} and finding the best fit to the measured binding energies.[15] The complex peak structure observed when ionising with 800 nm photons could be well resolved when ionising with pulse durations in the ps range and the peaks were assigned to three Rydberg series corresponding to angular momenta ℓ = 3, 5 and 7. In spite of the relatively good fit to the binding energies predicted by the simple model, the extracted quantum defects did not show typical Rydberg behaviour; the extracted quantum defect values were very large and did not change significantly, as expected, with principal quantum number n or angular momentum quantum number, ℓ.[50] In a recent study, using a combination of VMI angular-resolved PES with TD-DFT calculations,[16] it was found that the most prominent peaks can be assigned to single-photon ionisation of excited electronic states comprised of so-called "Superatom Molecular Orbitals" (SAMOs). These are diffuse hydrogenic orbitals bound to the hollow molecular core that were recently imaged in scanning tunnelling spectroscopy experiments on fullerenes deposited on a metal substrate.[49, 51] They are basically low-lying members of low angular momentum Rydberg series but differ from conventional Rydberg states due to the presence of an additional

shallow attractive potential that arises from electron correlation effects. The effect has been likened to that of an image charge potential at the surface of a metal.[49] The hollow cage structure typical of fullerenes thus leads to the presence of a shallow attractive potential inside the cage such that, for a low-lying *s*-SAMO the maximum of the probability density is actually localized inside the cage, Figure 9. As the principal quantum number increases, the SAMOs will converge to a conventional Rydberg series as the electron density is moved farther and farther away from the cage and the long-range Coulomb force dominates the interactions.

The SAMOs are thought to be of potential importance for technical applications since they form nearly-free-electron bands in solids.[49] Studying these states in the gas-phase offers an alternative approach to scanning tunnelling spectroscopy that is free from any substrate interactions and thus more amenable to a detailed comparison with theory and fundamental understanding of the factors that influence the binding energies. A key challenge is to reduce the energy gap between the HOMO and the SAMOs of hollow molecules to prepare suitable molecular building blocks for future electronics applications.[52]

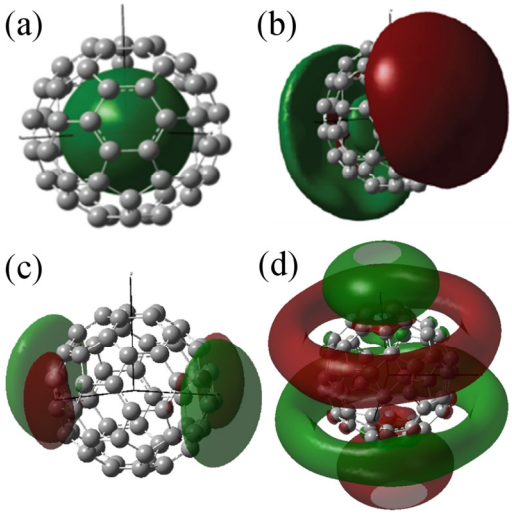

Figure 9: *Contour plots of the SAMOs corresponding to (a) s-, (b) p-, (c) d- and (d) f-symmetry from TDDFT calculations.[53] Figure kindly supplied by F. Remacle and B. Mignolet.*

The key to identifying the contribution of the SAMO states to the structure in the PES was the determination of the PADs.[16] One dominant peak, with a binding energy, E_{Bind} = 1.90 eV showed an angular distribution characterised by $\beta \approx 2.0$ for all photoelectron kinetic energies (i.e. suitable laser wavelengths, Figure 2) accessible in the laboratory. This dependence is expected from an *s*-state (Equation 2) and it was therefore hypothesised that the s-SAMO was contributing to the signal. A computational study, using time-dependent density function theory (TD-DFT), was able to clearly identify the SAMOs among the high density of excited states[53]. PADs were calculated for large bands of states around the identified SAMO states. The photoionisation widths (or cross sections) were found to be orders of magnitude larger for the diffuse SAMO states than for the neighbouring "non-SAMO" states with the electron densities centred on the carbon atoms of the cage.[53] The comparison of binding energies and PADs provided an assignment of the most prominent peaks in the PES, shown e.g. in Figure 10, to the 3*s*, 3*p*, 3*d* and 4*s* SAMOs (where *n* is related to the number of radial nodes in the electron wavefunction). The large difference in photoionisation cross-sections between the SAMO and non-SAMO excited states,[53] can explain the clear prominence of peaks due to single-photon ionisation of diffuse states, such as SAMOs or conventional Rydberg states, in the fs PES. The photoionisation cross-section for these states is so high that they will be photoionised as soon as they are populated as long as the laser pulse is still present. All other excited states have such a low photoionisation cross-section for the laser wavelengths investigated experimentally that the probability of their ionisation occurring within the ca. 100fs timescale of the laser pulse duration is vanishing small even if they have an equal or even higher probability of being populated. The low rate of photoionisation from the non-SAMO states may be the major factor behind the development of a high electron temperature with subsequent thermal electron emission as discussed in the previous section.

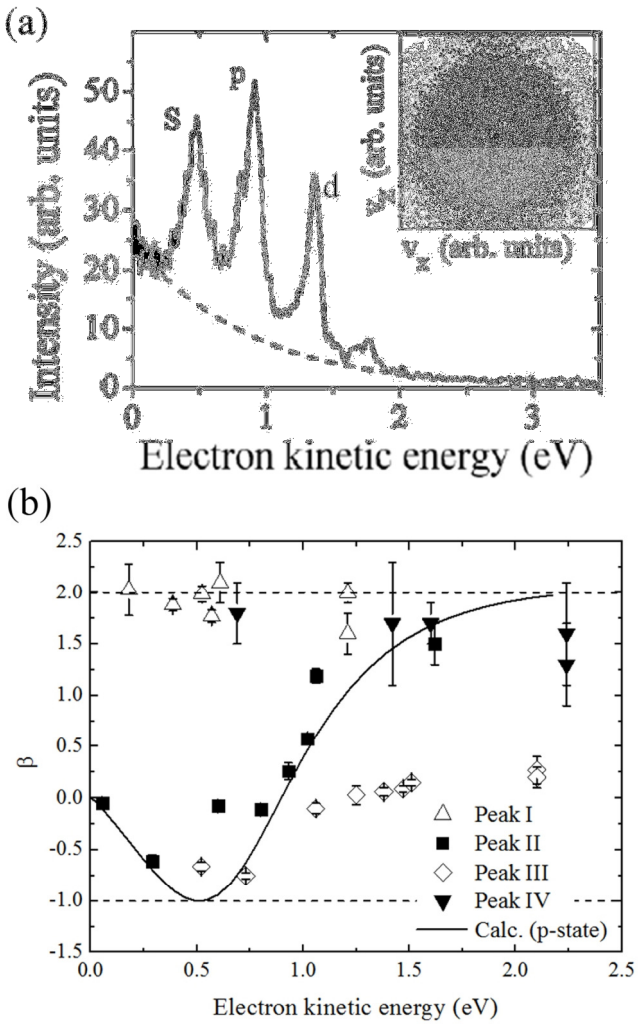

Figure 10: *(a) PES along the polarisation direction obtained using 90 fs, 532 nm excitation. The underlying thermal electron signal is plotted as a dashed line. The inset shows the VMI image. Adapted from J.O. Johansson et al., EPJ Web of Conferences* ***41****, 02015 (2013) (b) Anisotropy parameter extracted from SAMO PADs (I:3s, II: 3p, III: 3d, IV: 4s) and compared to the calculated results for the p-state. Reproduced with permission from Physical Review Letters 108, 173401 (2012), copyright American Institute of Physics (2012),*

Conclusions

Fullerenes are particularly interesting systems to probe the dynamics of electronic excited states since they conveniently bridge the gap between molecular and bulk-like behaviour. The recent introduction

of VMI and the availability of photoelectron angular distributions from laser photoionisation of fullerenes under different laser excitation conditions have provided more insight into the mechanisms leading to electron loss in complex molecular systems. Experimental measurements in combination with TDDFT calculations are beginning to clarify some of the questions that have been open since the early days of gas phase fullerene studies such as the co-existence of thermal electron emission and well-resolved peak structure in PES. The mechanisms discussed here are not only relevant for fullerenes but are applicable to a wide range of more complex molecules and nanoparticles. By understanding the properties of the model fullerene systems we can hopefully learn to control and manipulate the complex electron dynamics and tailor-make molecular systems for specific applications.

Acknowledgements

We gratefully acknowledge the contribution of a large number of collaborators to the work presented here, in particular Francoise Remacle, Benoit Mignolet, Klavs Hansen and Juraj Fedor. Financial support was provided from the Leverhulme Foundation (RPF-298 “PES of hollow nanomaterials”).

References

1. H. W. Kroto, J. Heath, S. C. O'Brien, R. F. Curl and R. E. Smalley, Nature **318**, 162-163 (1985).

2. W. Kratschmer, D. L. Lowell, K. Fostiropoulos and D. R. Huffman, Nature **347**, 354-358 (1990).

3. J. Nelson, Materials Today **14** (10), 462-470 (2011).

4. W. Hu, Y.-T. Tao and H. Sirringhaus, Physical chemistry chemical physics : PCCP **14**, 14097-14098 (2012).

5. K. Ohmori, Annual Review of Physical Chemistry **60**, 487-511 (2009).

6. V. V. Lozovoy, X. Zhu, T. C. Gunaratne, D. A. Harris, J. C. Shane and M. Dantus, Journal of Physical Chemistry A **112**, 3789-3812 (2008).

7. J. Andréasson, U. Pischel, S. D. Straight, T. A. Moore, A. L. Moore and D. Gust, Journal of the American Chemical Society **133** (30), 11641-11648 (2011).

8. E. E. B. Campbell and R. D. Levine, Annual Review of Physical Chemistry **51**, 65-98 (2000).

9. E. E. B. Campbell, G. Ulmer and I. V. Hertel, Physical Review Letters **67**, 1986 (1991).

10. J. U. Andersen, E. Bonderup and K. Hansen, Journal of Physics B: Atomic, Molecular and Optical Physics **35**, R1-R30 (2002).

11. E. E. B. Campbell, K. Hansen, K. Hoffmann, G. Korn, M. Tchaplyguine, M. Wittmann and I. V. Hertel, Physical Review Letters **84**, 2128-2131 (2000).

12. C. P. Schick and P. M. Weber, The Journal of Physical Chemistry A **105** (15), 3735-3740 (2001).

13. M. Tsubouchi, B. J. Whitaker, L. Wang, H. Kohguchi and T. Suzuki, Physical Review Letters **86** (20), 4500-4503 (2001).

14. J. L. Gosselin and P. M. Weber, The Journal of Physical Chemistry A **109** (22), 4899-4904 (2005).

15. M. Boyle, K. Hoffmann, C. P. Schulz, I. V. Hertel, R. D. Levine and E. E. B. Campbell, Physical Review Letters **87**, 273401 (2001).

16. J. O. Johansson, G. Henderson, F. Remacle and E. E. B. Campbell, Physical Review Letters **108**, 173401 (2012).

17. K. Hansen, K. Hoffmann and E. E. B. Campbell, The Journal of Chemical Physics **119**, 2513-2522 (2003).

18. J. O. Johansson, J. Fedor, M. Goto, M. Kjellberg, J. Stenfalk, G. G. Henderson, E. E. B. Campbell and K. Hansen, The Journal of Chemical Physics **136**, 164301 (2012).

19. P. F. Coheur, M. Carleer and R. Collin, Journal of Physics B: Atomic, Molecular and Optical Physics **29**, 4987-4995 (1996).

20. R. E. Haufler, Y. Chai, L. P. F. Chibante, M. R. Fraelich, R. B. Weisman, R. F. Curl and R. E. Smalley, Journal of of Chemical Physics **95**, 2197-2199 (1991).

21. K. Hansen, R. Müller, P. Brockhaus, E. E. B. Campbell and I. V. Hertel, Zeitschrift für Physik D Atoms, Molecules and Clusters **42**, 153-155 (1997).

22. J. D. Close, F. Federmann, K. Hoffmann and N. Quaas, Chemical Physics Letters **276** (5-6), 393-398 (1997).

23. C. Bordas, F. Paulig, H. Helm and D. L. Huestis, Review of Scientific Instruments **67**, 2257-2268 (1996).

24. A. T. J. B. Eppink and D. H. Parker, Review of Scientific Instruments **68** (9), 3477-3484 (1997).

25. V. Dribinski, A. Ossadtchi, V. Mandelshtam and H. Reisler, Review of Scientific Instruments **73** (7), 2634-2642 (2002).

26. G. A. Garcia, L. Nahon and I. Powis, Review of Scientific Instruments **75**, 4989-4996 (2004).

27. G. M. Roberts, J. L. Nixon, J. Lecointre, E. Wrede and J. R. R. Verlet, Review of Scientific Instruments **80** (5), 053104-053107 (2009).

28. X. Liang, M. G. Levy, S. Deb, J. D. Geiser, R. M. Stratt and P. M. Weber, Journal of Molecular Structure **978** (1–3), 250-256 (2010).

29. J. Cooper and R. N. Zare, J. Chem. Phys. **48**, 942-943 (1968).

30. K. L. Reid, Annual Review of Physical Chemistry **54**, 397-424 (2003).

31. R. Mabbs, E. R. Grumbling, K. Pichugin and A. Sanov, Chemical Society reviews **38**, 2169-2177 (2009).

32. M. Meckel, D. Comtois, D. Zeidler, A. Staudte, D. Pavičić, H. C. Bandulet, H. Pépin, J. C. Kieffer, R. Dörner, D. M. Villeneuve and P. B. Corkum, Science **320** (5882), 1478-1482 (2008).

33. C. I. Blaga, J. Xu, A. D. DiChiara, E. Sistrunk, K. Zhang, P. Agostini, T. A. Miller, L. F. DiMauro and C. D. Lin, Nature **483** (7388), 194-197 (2012).

34. A. Amrein, R. Simpson and P. Hackett, Journal of Chemical Physics **94** (6), 4663-4664 (1991).

35. B. Baguenard, J. C. Pinaré, F. Lépine, C. Bordas and M. Broyer, Chemical Physics Letters **352**, 147-153 (2002).

36. K. Hansen, E. E. B. Campbell and O. Echt, International Journal of Mass Spectrometry **252** (2), 79-95 (2006).

37. K. Hansen, *Statistical Physics of Nanoparticles in the Gas Phase*. (Springer, 2013).

38. K. Hansen, J. Chem. Phys. **128** (19), 194103 (2008).

39. P. Giannozzi and S. Baroni, Journal of Chemical Physics **100** (11), 8537-8539 (1994).

40. C. Bordas, B. Baguenard, B. Climen, M. A. Lebeault, F. Lépine and F. Pagliarulo, The European Physical Journal D - Atomic, Molecular, Optical and Plasma Physics **34**, 151-155 (2005).

41. F. Lépine, B. Climen, M. A. Lebeault and C. Bordas, Eur. Phys. J. D **55** (3), 627-635 (2009).

42. J. M. Weber, K. Hansen, M. W. Ruf and H. Hotop, Chemical Physics **239**, 271-286 (1998).

43. M. Kjellberg, O. Johansson, F. Jonsson, A. V. Bulgakov, C. Bordas, E. E. B. Campbell and K. Hansen, Physical Review A **81**, 23202 (2010).

44. A. Lassesson, K. Hansen, M. Joensson, A. Gromov, E. E. B. Campbell, M. Boyle, D. Pop, C. P. Schulz, I. V. Hertel, A. Taninaka and H. Shinohara, European Physical Journal D: Atomic, Molecular and Optical Physics **34**, 205-209 (2005).

45. R. Schlipper, R. Kusche, B. von Issendorff and H. Haberland, Applied Physics A: Materials Science & Processing **72**, 255-259 (2001).

46. M. Maier, M. Schätzel, G. Wrigge, M. Astruc Hoffmann, P. Didier and B. V. Issendorff, International Journal of Mass Spectrometry **252**, 157-165 (2006).

47. T. Laarmann, M. Rusek, H. Wabnitz, J. Schulz, A. R. B. de Castro, P. GÃ¼rtler, W. Laasch and T. Müller, Physical Review Letters **95** (6), 063402 (2005).

48. M. Kjellberg, A. V. Bulgakov, M. Goto, O. Johansson and K. Hansen, The Journal of Chemical Physics **133**, 074308 (2010).

49. M. Feng, J. Zhao and H. Petek, Science **320**, 359-362 (2008).

50. M. Boyle, T. Laarmann, K. Hoffmann, M. Hedén, E. E. B. Campbell, C. P. Schulz and I. V. Hertel, The European Physical Journal D - Atomic, Molecular, Optical and Plasma Physics **36** (3), 339-351 (2005).

51. M. Feng, J. Zhao, T. Huang, X. Zhu and H. Petek, Accounts of chemical research **44**, 360-368 (2011).

52. J. Zhao, M. Feng, J. Yang and H. Petek, ACS Nano **3**, 853-864 (2009).

53. B. Mignolet, J. O. Johansson, E. E. B. Campbell and F. Remacle, submitted (2013).